Dynamic Response Analysis of Steel-Concrete Beam Deck Pavement under Moving Load

Guofang Zhao[1], Jiaxin Hu[2], Qizhi Wang[3], Yongkang Yan[4] and Baoxing Gong[5,*]

[1]Department of Computer Technology, Hebei College of Institution and Technology, Shijiazhuang 050091, China
[2]Department of Civil & Environmental Engineering, Michigan State University, East lansing, Michigan 48825, America
[3]Department of Planning and Development, Shijiazhuang Expressway Group Co., Ltd, Shijiazhuang, 050800, China
[4]Faculty of Science, the University of Hong Kong, Hong Kong 999077, China
[5]School of Civil Engineering, Shijiazhuang Tiedao University, Shijiazhuang 050043, China

_____

Abstract

The dynamic stability and long-term safe operation of long span continuous beam bridge have potential safety hazards under the vehicle dynamic load. In order to explore the vibration characteristics of steel-concrete composite continuous bridge and study the dynamic response of pavement system of three-span steel-concrete composite continuous girder bridge under moving load.Based on the viscoelastic constitutive relation of asphalt mixture in bridge deck pavement, a three-dimensional numerical analysis model of three-span steel-concrete composite continuous beams was established by using ABAQUS finite element software. By writing the DLOAD and UTRACLOAD load subroutine to implement the vehicle moving load, the central difference method was applied to solve the deflection and stress of the three-span steel-hybrid continuous beam bridge at different vehicle speeds, and the stress state of each pavement layer of the bridge deck was compared and analyzed. The results show that the vertical deflection of the third span is the largest, the first span is the second, and the second span is the smallest under vehicle vibration load. The difference of vertical deflection of bridge deck is very small and can be ignored. With the increase of vehicle speed, the vertical deflection of pavement layer decreases. In addition, in terms of structural stress, the influence of vehicle vibration load on steel-concrete composite continuous beam bridge gradually decreases from top to bottom, and the mechanical characteristics of different structural parts are different. The conclusions obtained in this study can provide a theoretical basis for the design and construction of multi-span steel-composite continuous beam bridge.

Keywords: Moving load, Steel-concrete continuous beam, Dynamic response, Bridge deck pavement

_____

1. Introduction

Steel-concrete composite continuous beams, as important transverse load-bearing components in composite structural system, have broad application prospects in the fields of architecture and bridge structures. Compared with reinforced concrete structures, it has the advantages of light weight, good seismic performance, can reduce the cross-sectional size of components, and save cost; Compared with steel structure, it has the advantages of improving the stability, fire resistance and durability of components.

At present, domestic and foreign researches on multi span steel-concrete composite continuous girder bridges mostly focus on static properties such as bending resistance and shear resistance, while vehicle bridge coupling vibration response analysis and vibration control research are still at the stage of experience exploration and personalized research. There is a lack of research on the dynamic response characteristics and dynamic stability of bridge deck pavement structure under vehicle bridge coupling [1, 2].

With the continuous development of urban construction, traffic congestion is becoming increasingly severe. In order to relieve urban traffic pressure, steel-concrete composite continuous girder bridges have been widely used due to their advantages such as low gravity, large spanning capacity, and fast construction speed. However, under the long-term effect of vehicle traffic load, the bridge deck pavement system will have some problems, such as cracks, pelling, and rutting. Once rainwater soaks into the cracks, corrosion lesions will appear on the steel structure, which will affect the stability and durability of the steel-concrete composite continuous beam bridge. Therefore, it is of great significance to study the dynamic response of steel-concrete composite multi-span continuous beam bridges to ensure the safe operation and driving comfort of vehicle.

2. State of the art

Some scholars have partially studied the dynamic problem of the bridge deck pavement. For example, Hou et al. considered the slippage problem between steel beam and concrete slab, and analyzed the vibration characteristics of composite beams under moving loads [3]. Shaheen et al. established a three-dimensional vehicle model of the bridge, and solved the dynamic response of each node of the bridge according to the mechanical contact relationship between the vehicle and the bridge [4]. Based on the theory of transient heat conduction, Li & Ren obtained the structural mechanical response and deformation effect of steel box girder by using castable asphalt concrete with different spreading temperatures and thicknesses [5]. In order to study the influence of heavy load vehicles and temperature on epoxy asphalt mixture on the pavement of the bridge deck,

Li & Ren calculated the tensile stress of the surface of pavement layer by applying the moving load and the most unfavorable temperature on the steel bridge deck [6]. Remennikov et al. established 1/4 vehicle model of simply supported beam, and analyzed the the dynamic response of the bridge deck pavement under the random vehicle load [7]. Mirzaee et al. studied the damage of cyclic vehicle load and sustained temperature to the fatigue damage of the bridge deck pavement system by applying the damage mechanics theory [8]. Deng & Matsumoto established the simply-supported beam models with different spans and sections, and solved the variation of the dynamic impact coefficient of the bridge [9]. Greco & Lonetti analyzed the problem of vehicle-bridge dynamic coupling with virtual excitation method and separation iteration algorithm [10]. Nguyen et al. studied the dynamic responses of single, double and triple rear shafts to bridges [11]. Although there are many scholars have studied the dynamic coupling of vehicle and bridge, most of them simplified the vehicle load to be constant in the pavement system of bridge deck. Even though some experts analyzed the pavement of bridge deck in layers, they did not consider the actual properties of the pavement material (asphalt mixture) of bridge deck. Therefore, the existing researches can not objectively describe the actual stress-strain situation of vehicle-bridge under vibration load [12-20].

The finite element model of a three-span steel-concrete composite continuous beam was established in this study, and the viscoelastic constitutive relation of asphalt material was considered in the pavement system of the bridge deck. The vertical uniformly distributed moving load and 30% horizontal impact load were simultaneously applied on the bridge deck. The variation laws of the deflection and stress of the pavement of the three-span steel-concrete composite continuous beam bridge were solved with the central difference method, which provides the reference for the pavement design of the steel bridge deck in the future.

The rest of this study is organized as follows. Section 3 presents the proposed algorithm for network clustering in detail. Section 4 describes the experimental studies of the proposed method, and finally, the conclusions are summarized in Section 5.

3. Methodology

3.1 Pavement system of the continuous beam bridge deck
Taking a steel-concrete composite continuous beam bridge structure of an expressway as the prototype, a finite element model of steel-concrete composite continuous beam bridge (including bridge deck pavement structure layer) was established using ABAQUS finite element software, as shown in Fig. 1 [21, 22]. The bridge deck pavement structure was simplified into four layers: asphalt upper layer (SMA-13), asphalt lower layer (AC-20), C50 concrete and steel plate bottom layer. To prevent the concrete moving, the shear nail was set between the steel plate bottom layer and the concrete. In addition, the X-axis direction of the model was the transverse direction of the bridge, the *Z*-axis of the model was the longitudinal direction of the bridge, the *Y*-axis direction of the model was the direction perpendicular to the bridge deck. Constraints along the *x*, *y*, and *z* directions were imposed at the end of the first span of the continuous beam bridge, and constraints along the *x* and *y* directions were imposed at the rest of the bridge.

The length of steel-concrete composite continuous beam bridge was 90 m, which was divided into three spans, each span 30 m. The bridge deck had bidirectional and four lanes with a width of 11.88 m, and the longitudinal structure of the bridge was composed of four main longitudinal beams of I-beam. The height of the main longitudinal beam of I-beam was 1.65 m, and the spacing of the main longitudinal beam was 3.5 m. The finite element model of steel-concrete composite continuous beam bridge was divided into grids by using C3D8R eight node solid element [23]. To make the calculation more accurate, the grids where the moving load is applied should be properly encrypted.
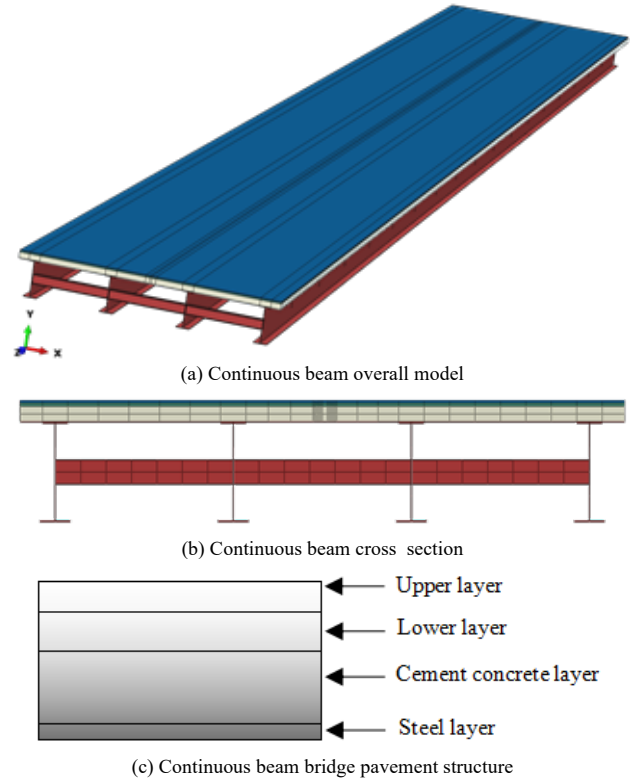

(a) Continuous beam overall model

(b) Continuous beam cross section

(c) Continuous beam bridge pavement structure
Fig. 1. Finite element model of three-span steel-concrete composite continuous beam (including bridge deck pavement structure).

The sheet layer, main longitudinal beam and short crossbeam were used with Q345D steel, which was a homogeneous, isotropic, linearly elastic material [24]. It was completely continuous between the layers of the bridge deck pavement, and the specific parameters of the bridge deck pavement are shown in Table 1.

The three-span steel-concrete composite continuous beam bridge were discretized by finite element method, and the vibration equation of the bridge can be written as:

$$[M]\ddot{Y}+[C]\dot{Y}+[K]Y = F \tag{1}$$

where, [*M*], [*C*], and [*K*] respectively represent the matrices of mass, damping and elastic stiffness. $\ddot{Y}$, $\dot{Y}$, and *Y* represent vectors of acceleration, velocity, and displacement respectively. *F* is the load vector.

When the dynamic equation of steel-concrete composite bridge is solved, RAYLEIGH damping hypothesis was used in the damping matri:

$$[C] = \alpha[M]+\beta[K] \tag{2}$$

where, *α* and *β* is damping coefficient.

They are determined by the following empirical formulas:

$$\alpha = \frac{2\omega_1\omega_2(\xi_1\omega_2 - \xi_2\omega_1)}{\omega_2^2 - \omega_1^2} \tag{3}$$

$$\beta = \frac{2(\xi_2\omega_2 - \xi_1\omega_1)}{\omega_2^2 - \omega_1^2} \tag{4}$$

where, ω_1 and ω_2 are the first two order inherent frequencies of the three-span steel-concrete composite continuous beam, which are calculated by ABAQUS modal analysis. ξ_1 and ξ_2 are the damping ratios of the first two order vibration modes. $\xi_1=\xi_2= 0.05$.

Table 1. Basic parameters of the steel-concrete continuous beam bridge.

Pavement layer structure	Thickness (mm)	Modulus of elasticity (MPa)	Poisson's ratio	Density (kg/m³)
Upper layer (SMA-13)	40	1400	0.35	2400
Lower layer (AC-20)	60	1200	0.20	2300
Cement concrete layer	250	2.95e5	0.20	2300
Steel bridge deck	15	2.10e5	0.30	7800
Longitudinal beam roof	20	2.10e5	0.30	7800
Longitudinal beam floor	25	2.10e5	0.30	7800

3.2 Selection of asphalt mixture parameters

The mechanical response of the asphalt mixture is closely related to temperature, load and time. The viscoelastic properties of asphalt materials are considered in the model of this paper, and the relaxation modulus of asphalt is determined through the transformation of viscoelastic relations of asphalt mixture, which is then imported into finite element software to define viscoelastic material. The time dependence of relaxation modulus is expressed as a sequence of shear modulus Prony series:

$$g(t) = g_0\left[\alpha_\infty^g + \sum_{i=1}^{n_g} \alpha_i^g \exp\left(-\frac{t}{\tau_i^g}\right)\right] \tag{5}$$

The shear modulus is:

$$g_\infty = g_0\alpha_\infty^g \tag{6}$$

$$g_i = g_0\alpha_i^g \tag{7}$$

The volume modulus is:

$$k_\infty = k_0\alpha_\infty^k \tag{8}$$

$$k_i = k_0\alpha_i^k \tag{9}$$

where, α_i^g and α_i^k are the relative moduli, g_0 and k_0 are the instantaneous moduli.

They are defined as follows:

$$g_0 = g(t=0) = g_\infty + \sum_i^{n_g} g_i \tag{10}$$

$$k_0 = k(t=0) = k_\infty + \sum_{i=1}^{n_k} k_i \tag{11}$$

When k_i values are all set to 0, the remaining parameters are as show in Table 2.

The temperature dependence of asphalt mixture has been calculated with the Williams-Landel-Ferry(WLF) equation:

$$\log(\alpha_T) = \frac{-C_1(T-T_r)}{C_2 + (T-T_r)} \tag{12}$$

where, α_T is the time-temperature displacement factor, C_1 and C_2 are regression coefficients, T is the test temperature, and T_r is the reference temperature.

Table 2. Asphalt mixture Prony parameters.

Parameter t_i	Parameter q_i	
	SMA-13	AC-20
0.00001	0.7490	0.3933
0.0001	0.1063	0.2357
0.001	0.0643	0.1867
0.01	0.0290	0.1168
0.1	0.0145	0.0438
1	0.0068	0.0153
10	0.0036	0.0044
100	0.0017	0.0007
1000	0.0013	0.0018

The parameters of (WLF) equation[25, 26] are shown in Table 3.

Table 3. Relaxation Variable (WLF) Equation Parameters.

Material type	T_r	C_1	C_2
Upper layer (SMA-13)	20	27.5	288.8
Lower layer (AC-20)	20	32.7	268.9

Asphalt pavement is simulated by generalized Maxwell model, while other pavement materials of the bridge deck are simulated by linear elastic constitutive model in this study.

3.3 Realization of the moving load

The moving load in this model was single axle and double wheel group, and the double round load was equivalent to the rectangular load to facilitate calculate process, as shown in Fig. 2(a). The length of the load was 0.2 m and the width was 0.184 m. Single-axle twin-wheel couple 100 kN was used as standard axle load, the single wheel load was 25 kN, and the grounding pressure was 0.7 MPa. In addition, the driving load was simplified into vertical load and 30% horizontal impact load, and the vertical load was input by subroutine DLOAD, while the horizontal load was input by subroutine UTRACLOAD. Detailed load application diagram is shown in Fig. 2(b). Considering the non-linearity of the asphalt mixture, the central difference method was used to solve the model [27, 28].

3.4 Model validation

To verify the accuracy and rationality of the moving load, the field test results were compared with the simulation results. The test site of a three-span steel-concrete composite

continuous beam is shown separately in Fig. 3. The test vehicle had a capacity of 50 tons, and the parameters of truck are shown in Table 4. The three-axle vehicle was used for numerical simulation, and the schematic diagram of the loading area is shown in Fig. 4. The six rectangles in Fig. 4 are used to represent vehicle loads, when the vehicle speed is 50 km/h, the comparison between the experimental and simulated values of the vertical

Length of vehicle head	2.4 m
Height of vehicle head	1.75 m
Distance between front and rear axes	4.3 m
Distance between two rear axes	1.37 m
Distance between two front axle wheels	2.20 m
Distance between center of two wheels on the same side of the same rear axle	0.36 m

(a) Rectangular load diagram

(b) Loading method
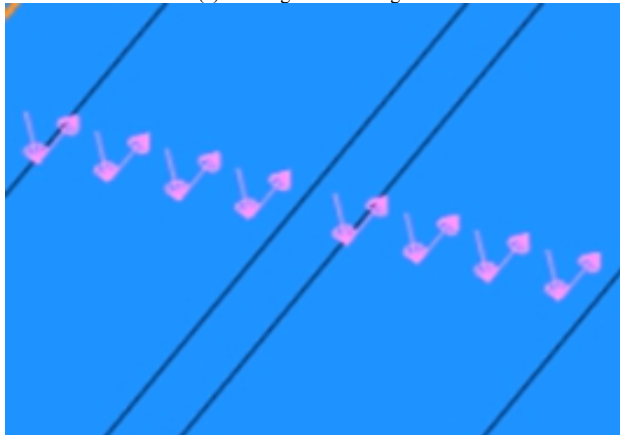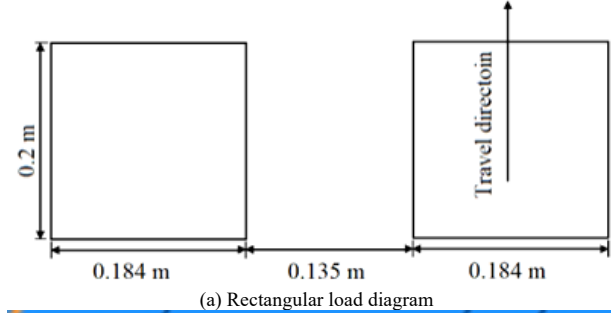
Fig. 2. Double wheel rectangular load.

deflection of the continuous beam is shown in Fig. 5.

(a) Field test vehicle   (b) Non contact measuring instrument

(c) Trip test   (d) Modal test

Fig. 3. Test site photos.

Table 4. Three-axle truck parameters.

| Vehicle size	Value
Weight of empty vehicle	18.5 t
Front axle weight of empty vehicle	6.5 t
Double rear axle weight of empty vehicle	12 t
Weight of fully loaded vehicle	50 t
Front axle weight of fully loaded vehicle	9.8 t
Double rear axle weight of fully loaded vehicle	40.2 t
Length of vehicle body	6.5 m
Width of vehicle body	2.5 m
Height of vehicle body	1.9 m
Width of vehicle head	2.3 m
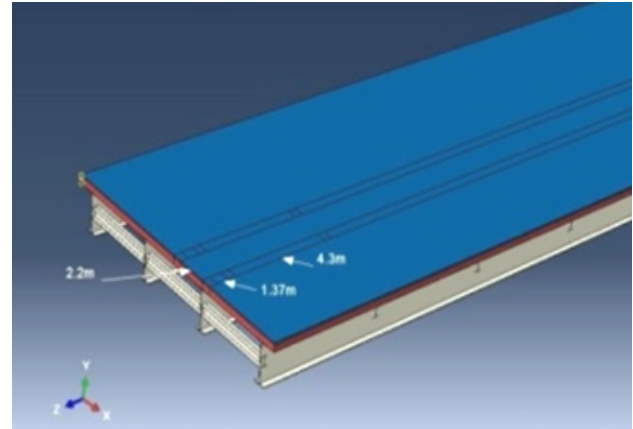
Fig. 4. Simulation load area layout.
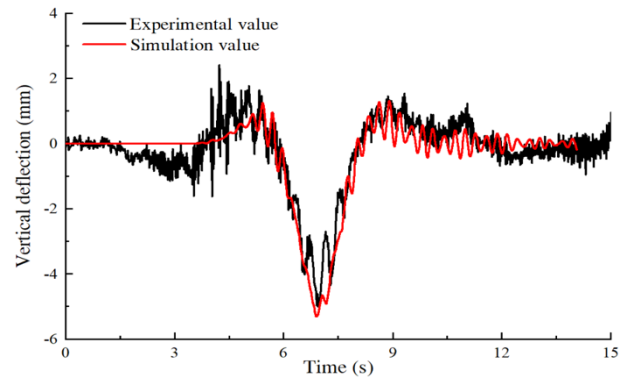
Fig. 5. Comparison of vertical deflection between test and simulation

Due to the test conditions are very complex and the experiment is affected by many factors, such as the external environment, vehicle speed and the location of the sampling point, etc. There is a certain error between the test value and the simulation value, and the specific value of the error is shown in Table 5. The comparison of test frequency and simulation calculation frequency is shown in Table 6.

Table 5. Vertical maximum deflection of second span of the beam.

Vehicle speed (km/h)	Vertical deflection value (mm)		
	Test value	Simulation value	Error (%)
15	5.81	6.2	6.7
25	5.46	5.78	5.9
40	4.98	5.2	4.4
50	4.89	5.2	6.3

Table 6. Comparison of frequency between test and simulation

Measured order	Measured value (Hz)	Calculated value (Hz)	Error%
First order	3.516	3.3452	4.8
Second order	4.102	4.1726	1.7
Third order	4.980	5.3560	7.5

In Table 5, the variation trend of the vertical deflection measured in the field is almost the same as that of the simulation results. The vertical deflection of the numerical simulation is slightly larger than that of the field

measurement. The error between the calculated and experimental values of the first order frequency of a three-span steel-concrete composite continuous beam is 4.8%, and the difference is 1.7% for the second order frequency and 7.5% for the third order frequency. The main reason for the frequency error is that some optimizations have been added to the model of the three-span steel-composite continuous beam bridge rather than to the structure of the actual bridge. However, the error does not affect the overall effect. In summary, the mechanical characteristics of continuous beam in the finite element model in this paper are basically consistent with the field measured results. Therefore, all of the above prove that the data is reasonable.

3.5 Roughness of steel deck pavement

When the coupling effect of the vehicle-bridge is studied, the road roughness can cause vehicle vibration, so it must be considered. The road roughness in this paper is expressed by the road power spectral density $G_q(n_0)$ in Chinese GB/T7031-8 (Vehicle Vibration Input-Road Roughness Representation Method).

$$G_q(n) = G_q(n_0)\left(\frac{n}{n_0}\right)^{-w} \tag{13}$$

where, n is the spatial frequency, n_0 is the reference space frequency, let $n_0 = 0.1$ m^{-1}. $G_q(n_0)$ is the coefficient of road roughness. w is the frequency exponent, usually $w = 2$.

The pavement roughness is calculated by the random phase cosine superposition method, and the specific formula is as follows:

$$r(x) = \sum_{i=1}^{N}\sqrt{4G(n_i)\Delta n}\cos(n_i x + \theta_i) \tag{14}$$

where, $r(x)$ is the roughness of the bridge deck. x is the vertical position of the bridge deck. $G(n_i)$ is the power spectral density function. n_i is a spatial frequency, Δn is frequency increment. θ_i is the random phase angle, which uniformly distributed between 0-2π.

In order to increase the effect of vehicle vibration, the poor Grade-C road surface was used to analyze in this study. The road roughness coefficient is 256e^{-6}, and the curve of pavement irregularities of Grade-C bridge deck was calculated by MATLAB/ Simulink modeling [29, 30].

4. Results analysis and discussion

4.1 Displacement response of the pavement of the continuous beam bridge

4.1.1 Comparison of the vertical deflection of the upper layer

When the moving speed is 20 m/s, the vertical deflection of the three spans of the three-span steel-concrete composite continuous beam differ greatly in Fig. 6. The vertical deflection of the upper layer in the mid-span of the first span, second span and third span is 0.59 mm, 0.56 mm and 0.68 mm, respectively. The third span has the greatest vertical deflection, followed by the first span and the second span with the smallest, and the difference between the maximum deflection and the minimum deflection is 0.12 mm.
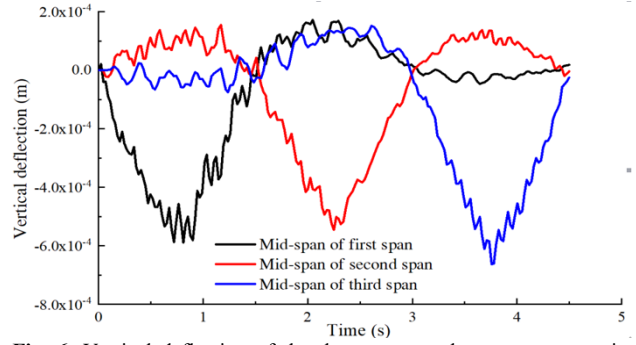

Fig. 6. Vertical deflection of the three-span steel-concrete composite continuous beam.

4.1.2 Vertical deflection comparison of each pavement layer of bridge deck

Vertical deflection curve of each span pavement in the three-span steel-concrete composite continuous beam bridge is shown in Figs. 7 to 9.

When the moving load acts, the vertical deflection of each span of the continuous beam pavement varies greatly, as shown in Figs. 7 to 9. The vertical deflection of the first span of the continuous beam fluctuates greatly. The vertical deflection of the main longitudinal beam in the first span is the smallest, followed by the short beam. The vertical deflection values of the upper layer, lower layer, cement concrete layer and steel plate layer in the deck pavement system are almost the same, larger than that of the main longitudinal beam and short beam. The vertical deflection of the second span of the continuous beam fluctuates slightly. The vertical deflection of the main longitudinal beam of the second span is the smallest, followed by the short beam, and the vertical deflection of the bridge deck pavement is the largest. The vertical deflection of the main longitudinal beam in the third span is the smallest, followed by the short beam. The bridge deck pavement has the greatest vertical deflection.
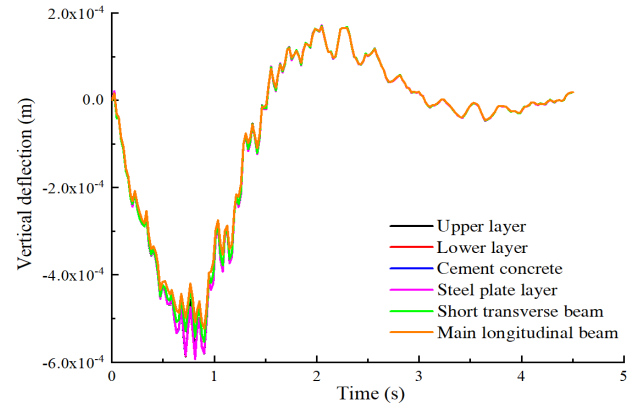

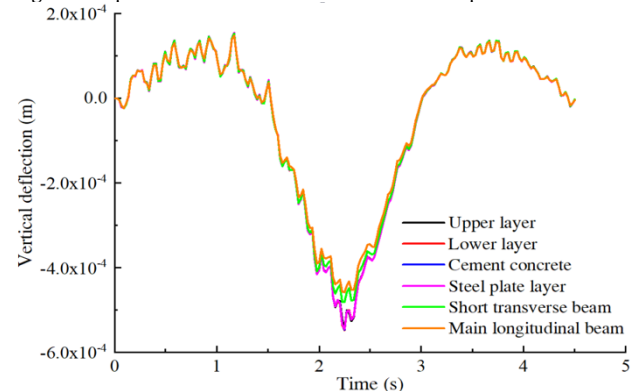**Fig. 7.** Comparison of vertical deflection of the first span.

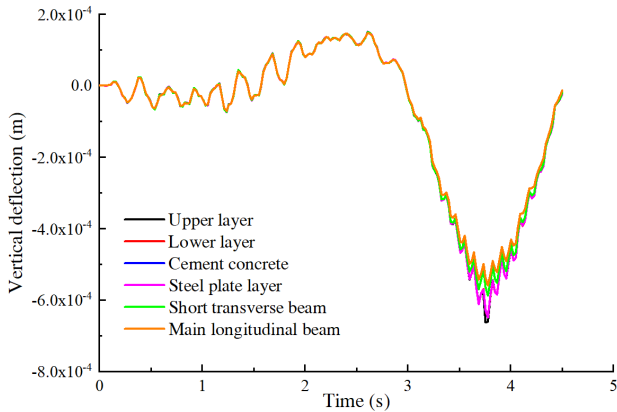**Fig. 8.** Comparison of vertical deflection of the second span.

Fig. 9. Comparison of vertical deflection of the third span.

4.1.3 Comparison of the deflection at different speeds

The vertical deflection curves of the second span of the three span steel-concrete composite continuous beam are shown in Figs. 10 and 11.

Under the moving load, the vertical deflection of the second span of the continuous beam varies in a complex way, as shown in Figs. 10 and 11. When the velocity of moving load is 10 m/s, 20 m/s, 30 m/s, 40 m/s, the vertical deflection value is 0.585 mm, 0.545 mm, 0.566 mm, 0.542 mm, respectively. From these data, the vertical deflection of the continuous beam does not decrease with increasing speed, when With the increase of the moving speed from 20 m/s to 30 m/s, the vertical deflection of the continuous beam increases slightly. But when the velocity increas from 30 m/s to 40 m/s, the vertical deflection of the continuous beam decreases gradually.
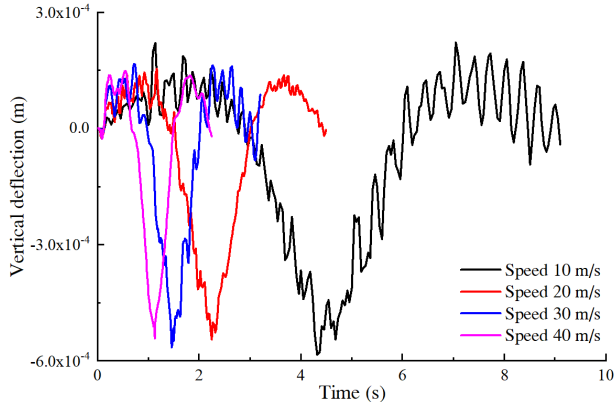
Fig. 10. Comparison of vertical deflection at different speeds.
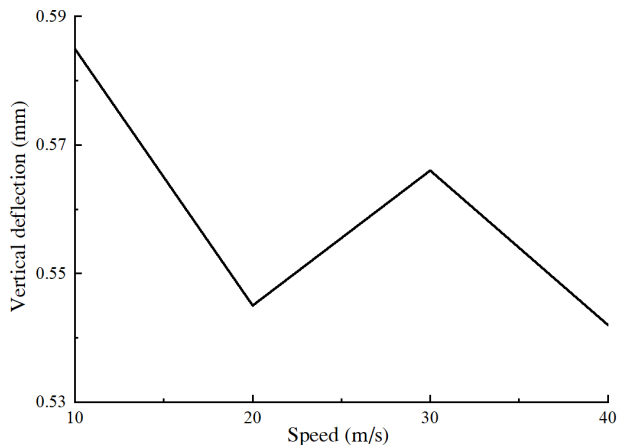
Fig. 11. Comparison of maximum deflection at different speeds.

4.2 Stress response of bridge deck pavements

4.2.1 Vertical stress analysis of bridge deck pavement

Vertical stress variation curves of each pavement layer of bridge deck are shown in Figs. 12 and 13. The vertical stress of the bridge deck pavement of the three-span steel-concrete composite continuous beam bridge is mainly compressive stress, the maximum value of which in the upper layer is 0.641 MPa, as shown in Fig. 12. The stress condition is very complex in the lower layer, which bears both compressive stress and tensile stress, and the vertical stress of the lower layer fluctuates a little. The maximum compressive stress of the lower layer is 0.51 MPa, and the maximum tensile stress of which is 0.078 MPa. The cement concrete layer is mainly subjected to compressive stress, and the maximum value is 0.257 MPa. The steel plate layer at the bottom is mainly subjected to compressive stress, with the maximum value of 0.041 MPa.
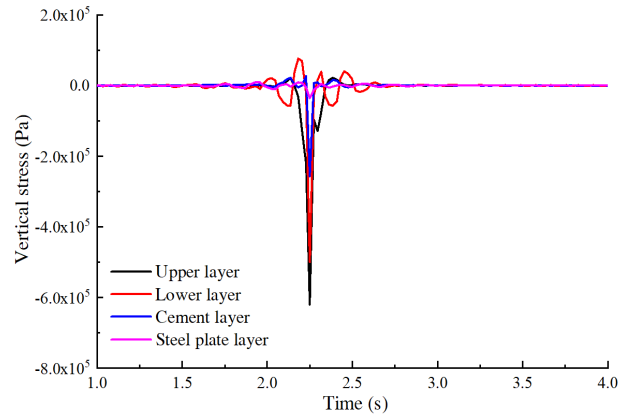

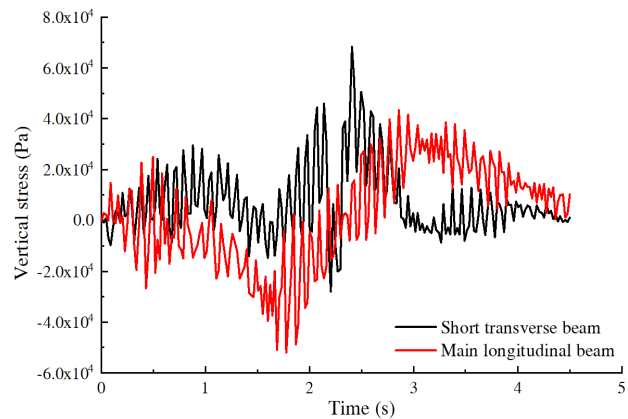**Fig. 12.** Comparison of vertical stress of pavement layer.

Fig. 13. Comparison of vertical stress between main longitudinal beam and transverse beam.

As can be seen from Fig. 13, the vertical stress of the main longitudinal beam includes both compressive stress and tensile stress. The vertical stress of the main longitudinal beam varies with time, the maximum compressive stress is 52.1 kPa, and the maximum tensile stress is 42.3 kPa. In addition, the vertical stress of the short beam also varies with time. Short beams also bear both compressive and tensile stresses, and the maximum compressive stress is 29.1 kPa and the maximum tensile stress is 68.2 kPa.

4.2.2 Transverse stress analysis of bridge deck pavement

The varied curve of the transverse stress of each pavement layer of bridge deck is shown in Figs. 14 to 17.

The transverse stress variation of each pavement layer of bridge deck is very complex, and most of the transverse

stress of the pavement layer is compressive stress, as shown in Fig. 14. The transverse stress curve of the upper layer presents symmetrical distribution characteristics, and the maximum compressive stress is 0.287 MPa. The transverse stress of the lower layer fluctuates greatly, bearing both compressive stress and tensile stress, and the maximum compressive stress is 0.302 MPa and the maximum tensile stress is 0.132 MPa. The main transverse stress of the cement concrete layer is compressive stress, and the maximum value of which is 0.265 MPa. The transverse stress curve of the cement concrete layer is distributed symmetrically.
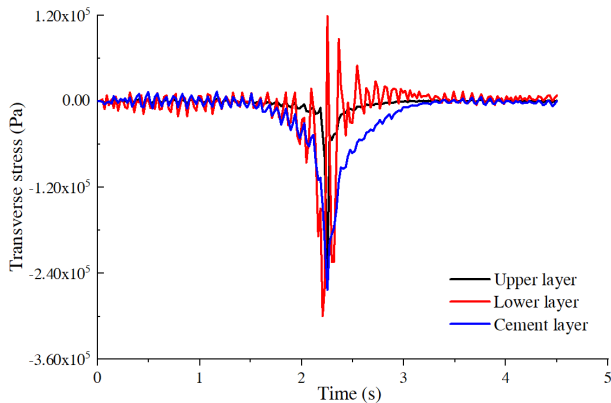
Fig. 14. Comparison of transverse stress of bridge pavement.

As can be seen from Fig. 15, the transverse stress of the steel plate layer is mainly tensile stress, and the maximum value is 3.02 MPa. The transverse stress curve of the steel plate is symmetrically distributed. As can be seen from Fig. 16, the transverse stress of the short beam is mainly compressive stress, with a maximum value of 0.374 MPa. The transverse stress curve is symmetrically distributed and has a certain fluctuation. As can be seen from Fig. 17, the transverse stress of the main longitudinal beam at the bottom of the continuous beam bridge is complex, and the main longitudinal beam bears both compressive and tensile stresses. In addition, the transverse stress varies with time, and the maximum compressive stress is 67.5 kPa and the maximum tensile stress is 67.5 kPa.
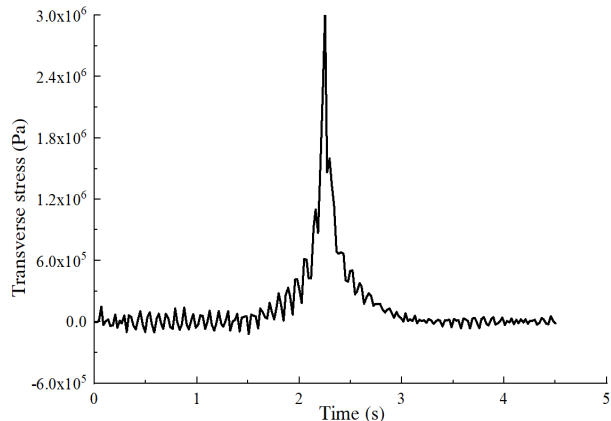
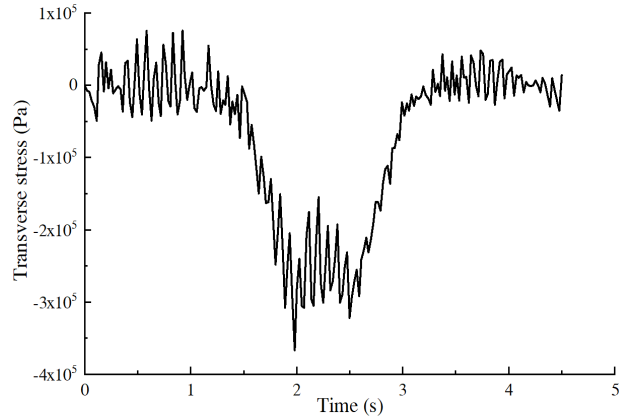Fig. 15. Comparison of transverse stress of steel plate layer.

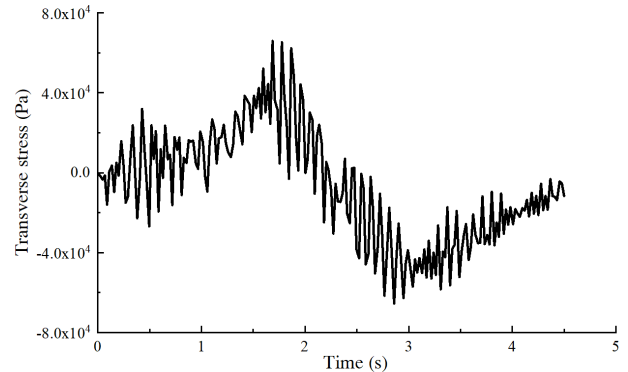Fig. 16. Comparison of transverse stresses of transverse beams.

Fig. 17. Comparison of transverse stress of main longitudinal beam

4.2.3 The longitudinal stress analysis of each pavement layer of the bridge deck

The varied curves of longitudinal stress of each pavement layer of the bridge deck are shown in Figs. 18 to 21.

As can be seen from Fig. 18, the longitudinal stress of the pavement layer is relatively complex. The upper layer is mainly subjected to compressive stress, and its maximum value is 0.183 MPa. The longitudinal stress curves of the upper layers are symmetrically distributed. The lower layer is subjected to both compressive and tensile stresses. The maximum compressive stress is 0.072 MPa and the maximum tensile stress is 0.192 MPa. Cement concrete layer is mainly subjected to compressive stress, and the maximum value is 0.241 MPa. The longitudinal stress curve of the cement concrete layer is symmetrically distributed.
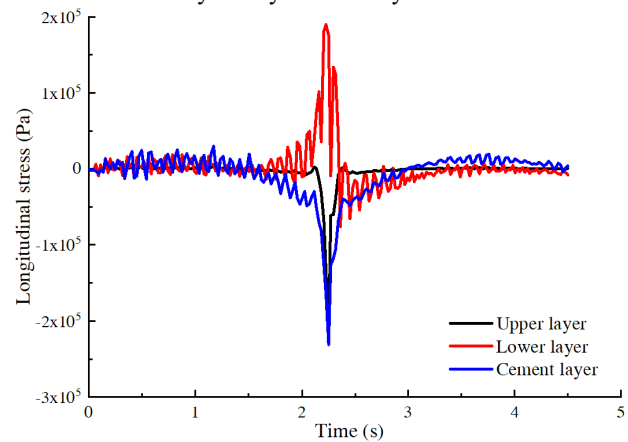
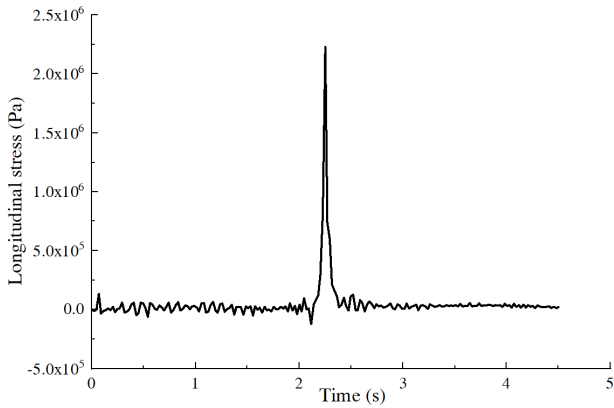Fig. 18. Comparison of longitudinal stress of pavement layer.

Fig. 19. Comparison of longitudinal stress of steel plate layer.

In Fig. 19, the steel plate layer at the bottom of the continuous beam bridge mainly bears tensile stress, with a maximum value of 2.24 MPa. The longitudinal stress curve of steel plate is symmetrically distributed.
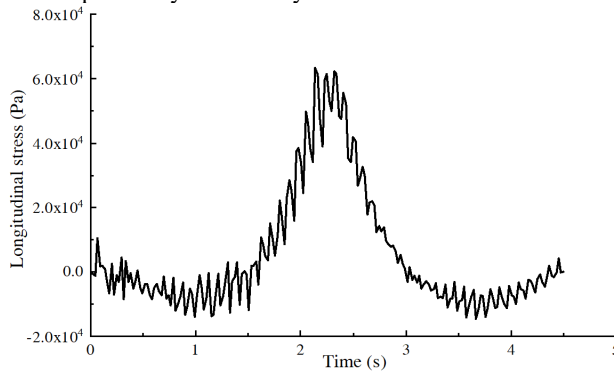

Fig. 20. Comparison of longitudinal stress of transverse beams.

The longitudinal stress of the short beam includes compressive stress and tensile stress, as shown in Fig. 20. The short beam is in the state of compression during the time period (0-1.5 s), in the state of tension during the time period (1.5 s-3 s), and in the state of compression during the time period (3 s-4.5 s). The maximum compressive stress of the short beam is 15.82 kPa and the maximum tensile stress is 64.75 kPa. The longitudinal stress curve of the short beam is symmetrically distributed. The tensile stress of the short beam is much greater than the compressive stress on it.
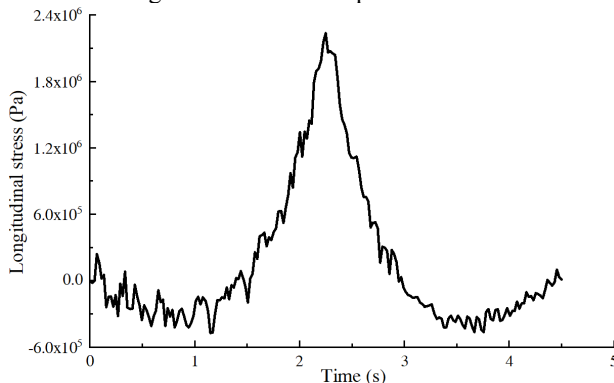

Fig. 21. Comparison of longitudinal stress of main longitudinal beam.

The longitudinal stress of the main longitudinal beam includes compressive stress and tensile stress, as shown in Fig. 21. The main longitudinal beam is in the state of compression during the time period (0-1.5 s), in the state of tension during the time period (1.5 s-3 s), and in the state of compression during the time period (3 s-4.5 s). The tensile stress of the main longitudinal beam is much greater than the

compressive stress. The maximum compressive stress of the main longitudinal beam is 0.498 MPa, and the maximum tensile stress is 2.24 MPa. The longitudinal stress curve of the main longitudinal beam is symmetrically distributed.

4.2.4 Stress nephogram
The stress nephogram of the bottom layer of the steel plate is shown in Figs. 22 to 24. The stress on the steel plate layer is more complex as shown in the Figs. 22 to 24. In the direction of S11 and S33, the stress nephogram is elliptical, and the stress at the center of the ellipse is maximum. In the direction of S13, the stress has both negative and positive values, which indicates that the steel plate layer is both tensile and compressive in the direction of S13.
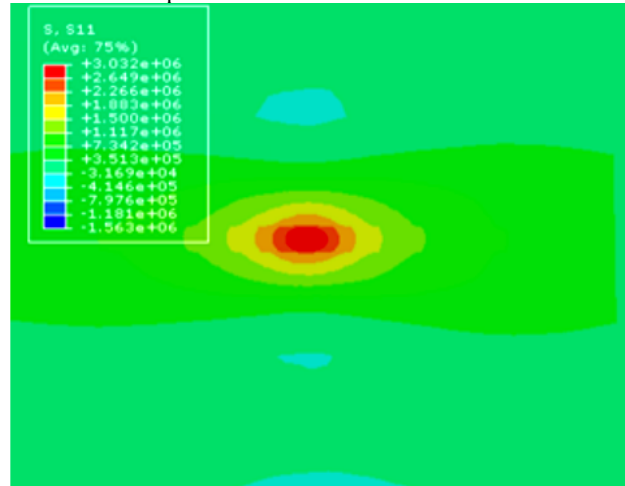

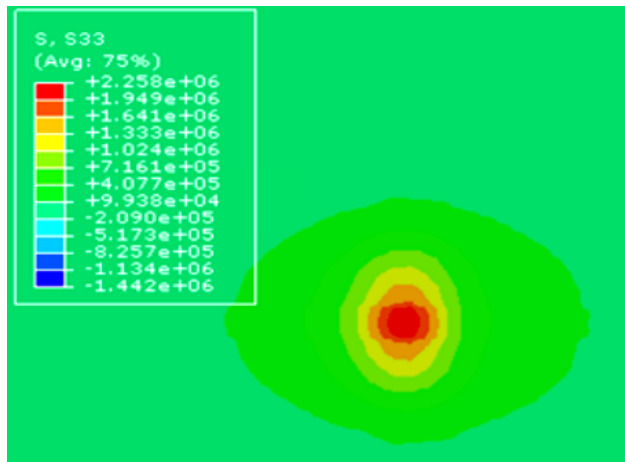**Fig. 22.** S11 stress nephogram of the steel plate layer.

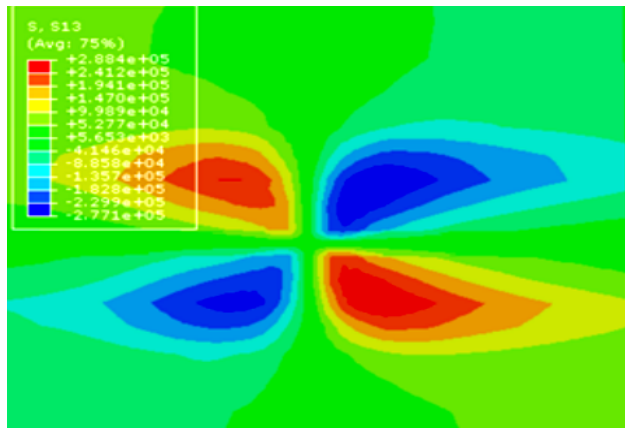**Fig. 23.** S33 stress nephogram of the steel plate layer.

Fig. 24. S13 stress nephogram of the steel plate layer.

4.3 Influence of vehicle axle load on response of steel deck pavement

To analyze the influence of vehicle axle load on the bridge deck pavement, taking the speed of 20 m/s as an example, the vertical deflection of the bridge deck pavement layer under different axle loads, as shown in Fig. 25. As can be seen from Fig. 25, the vehicle load has a great influence on the vertical deflection of the three-span continuous beam bridge. When the vehicle axle load is 25 kN, the vertical deflection of the second span of the continuous beam bridge is 0.545 mm. When the vehicle axle load is 30 kN, the vertical deflection of the second span of the continuous beam bridge is 0.644 mm, which increases by 18.2%. When the vehicle load is 40 kN, the vertical deflection of the second span of the continuous beam is 0.824 mm, which increases by 28%. These data show that the greater the axle load of the vehicle, the greater the vertical deflection.
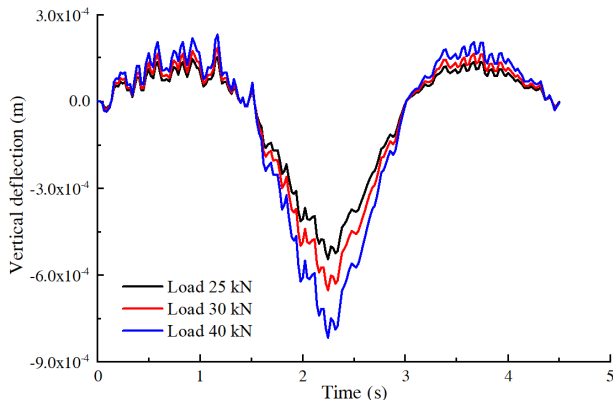

Fig. 25. Vertical deflection of the bridge deck pavementt under different axle loads.

As can be seen from Fig. 26, when the vehicle axle load is 25 kN, the transverse stress of the second span of the continuous beam is 0.247 MPa. When the vehicle axle load is 30 kN, the transverse stress of the second span of the continuous beam is 0.294 MPa, which increases by 19%. When the axle load of the vehicle is 40 kN, the transverse stress of the second span of the continuous beam is 0.365 MPa, which increases by 24.1%. These data show that the larger the axle load of the vehicle, the larger the transverse stress.
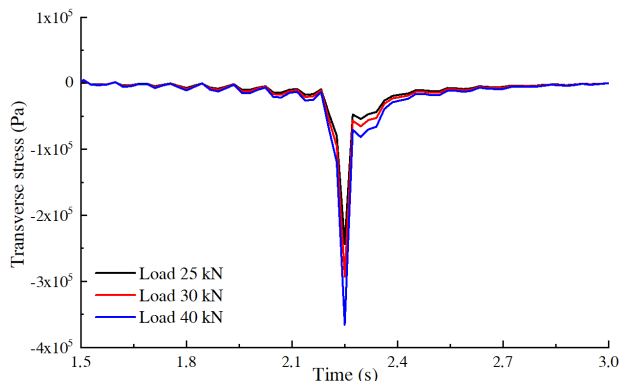

Fig. 26. Transverse stress of the bridge deck pavement under different axle loads.

As can be seen from Fig. 27, when the vehicle axle load is 25 kN, the longitudinal stress of the second span of the continuous beam is 0.224 MPa; when the vehicle axle load is 30 kN, the longitudinal stress of the second span of the continuous beam is 0.264 MPa, which increases by 17.9%. When the vehicle axle load is 40 kN, the longitudinal stress

of the second span of the continuous beam is 0.335 MPa, which increases by 26.9%. The above data indicate that the larger the axle load of the vehicle, the greater the longitudinal stress.
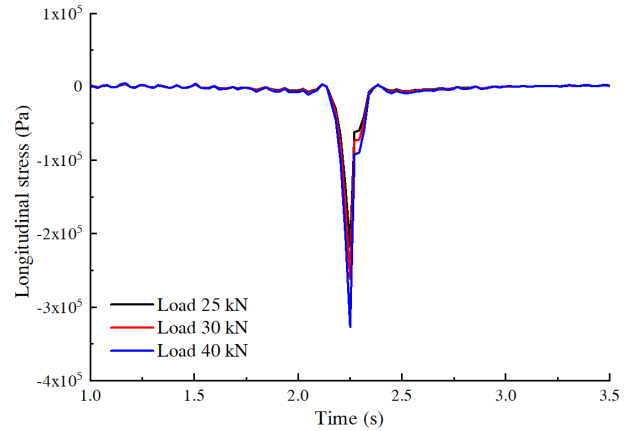

Fig. 27. Longitudinal stress of the bridge deck pavement under different axle loads.

5. Conclusions

The finite element model of a three-span steel-concrete composite continuous beam bridge was established and the viscoelasticity of bitumen material was considered in bridge deck paving material. The dynamic response of the pavement system of the continuous beam bridge under moving load was calculated using the central difference method. The main conclusions are obtained as following:

(1) Under the action of moving load, the vertical deflections of the three-span steel-concrete composite continuous beams are quite different. The vertical deflection of the third span is the largest, followed by the first span, the second span is the smallest. With the increasing axle load of the vehicle, the vertical deflection, lateral stress and longitudinal stress all increase by more than 20%.

(2) Under the action of moving load, the vertical deflection of the main longitudinal beam of the three-span steel-concrete composite continuous beam bridge is the smallest, followed by the short beam, the vertical deflection of the deck pavement layer (including the upper layer, the lower layer, the cement concrete layer and the steel plate layer) is the largest. In addition, the vertical deflection of the three-span steel-concrete composite continuous beam does not decrease with the increase of the moving speed, but increases to a certain extent when the moving speed is 30 m/s.

(3) The vertical stress of the bridge deck pavement is compressive stress, and the vertical stresses on the main longitudinal beam and short beam are compressive stress and tensile stress. The transverse stress of the upper and lower layers is mostly compressive stress. The transverse stress of the steel plate is mainly tensile stress, but that of short beam is mainly compressive stress. The main longitudinal beam bears both compressive and tensile stress. The longitudinal stress of the upper layer and the cement concrete layer is mainly compressive stress. The lower layer bears both compressive stress and tensile stress, while steel plate layer, short beam and main longitudinal beam mainly bear tensile stress. The tensile stress of the main longitudinal beam is much greater than that of the short beam.

Although this study has made some progress, due to the complexity of the actual engineering, considering the actual engineering conditions, the related work still needs to be analyzed in further.

Acknowledgements

_____

References

1. Zou, Y., Zhou, X. H., Di, J. "Partial interaction shear flow forces in simply supported composite steel-concrete beams". *Advanced Steel Construction*, 14(4), 2018, pp. 634-650.
2. Jeong, B., Kim, T., Lee, U. "Vibration analysis of a multi-span beam subjected to a moving point force using spectral element method". *Structural Engineering and Mechanics*, 65(3), 2018, pp. 263-274.
3. Hou, Z. M., Xia, H., Wang, Y. Q. "Dynamic analysis and model test on steel-concrete composite beams under moving loads". *Steel and Composite Structures*. 18(3), 2015, pp. 565-582.
4. Shaheen, M. A., Tsavdaridis, K. D., Yamada, S. "Comprehensive fe study of the hysteretic behavior of steel-concrete composite and noncomposite rws beam-to-column connections". *Journal of Structural Engineering*, 144(9), 2018, pp. 2124.
5. Li, S. H., Ren, J. Y. "Analytical study on dynamic responses of a curved beam subjected to three-directional moving loads". *Applied Mathematical Modelling*, 58, 2018, pp. 365-387.
6. Li, S. H., Ren, J. Y. "Investigation on three-directional dynamic interaction between a heavy-duty vehicle and a curved bridge". *Advances in Structural Engineering,* 21(5), 2018, pp. 721-738.
7. Remennikov, A. M., Kong, S. Y., Uy, B. "The response of axially restrained non-composite steel-concrete-steel sandwich panels due to large impact loading". *Engineering Structures*, 49, 2013, pp. 806-818.
8. Mirzaee, A., Abbasnia, R., Shayanfar, M. "Simultaneous identification of damage in bridge under moving mass by adjoint variable method". *Smart Structures and Systems*, 21(4), 2018, pp. 449-467.
9. Deng, P. G., Matsumoto, T. "Determination of dominant degradation mechanisms of RC bridge deck slabs under cyclic moving loads". *International Journal of Fatigue*, 112(7), 2018, pp. 328-340.
10. Greco, F., Lonetti, P. "Numerical formulation based on moving mesh method for vehicle-bridge interaction". *Advances in Engineering Software*, 121, 2018, pp. 75-83.
11. Nguyen, K., Velarde, C., Goicolea, J. M. "Analytical and simplified models for dynamic analysis of short skew bridges under moving loads". *Advances in Structural Engineering*, 22(9), 2019, pp. 2076-2088
12. Wang, S. R., Shi, K. P., He, Y. S., Wang, X. Q. "Dynamic response analysis of middle pillar for ultra-small spacing tunnels under train vibration loads". *Journal of Engineering Science and Technology Review*, 12(3), 2019, pp. 30-37.
13. Luo, T., Wang, S. R., Zhang, C. G., Liu, X. L. "Parameters deterioration rules of surrounding rock for deep tunnel excavation based on unloading effect". *DYNA*, 92(6), 2017, pp. 648-654.
14. Wang, S. R., Shi, K. P., Zou, Y. F., Zou, Z. S., Wang, X. C., Li, C. L. "Size effect analysis of scale test model for high-speed railway foundation under dynamic loading condition". *Tehnicki Vjesnik-Technical Gazette*, 28(5), 2021, pp. 1615-1625.
15. Wang, S. R., Liu, Z. W., Qu, X. H., Fang, J. Bo. "Large deformation mechanics mechanism and rigid-gap-flexible-layer supporting technology of soft rock tunnel". *China Journal of Highway and Transport*, 22(6), 2009, pp. 90-95.
16. Pisačić, K., Horvat, M., Botak, Z. "Finite difference solution of plate bending using Wolfram Mathematica". *Technical Journal*, 13(3), 2019, pp. 241-247.
17. Wang, S. R., Shi, K. P., Zou, Y. F., Zou, Z. S., Wojciechowski, A. "Coupling deformation between non-uniform settlement of track-structure and subgrade of high-speed railway above the mind-out areas". *Acta Montanistica Slovaca*, 26(4), 2021, pp. 620-633.
18. Wu, X. G., Wang, S. R., Yang, J. H., Zhao, J. Q., Chang, X. "Damage characteristics and constitutive model of lightweight shale ceramsite concrete under static-dynamic loading". *Engineering Fracture Mechanics*, 259, 2022, pp. 108137.
19. Wang, S. R., Zhao, J. Q., Wu, X. G., Yang, J. H., Liu, A. "Meso-scale simulations of lightweight aggregate concrete under impact loading". *International Journal of Simulation Modelling*, 20(2), 2021, pp. 291-302.
20. Wang, S. R., Wu, X. G., Yang, J. H., Zhao, J. Q., Kong, F. L. "Mechanical behavior of lightweight concrete structures subjected to 3D coupled static-dynamic loads". *Acta Mechanica*, 231(11), 2020, pp. 4497-4511.
21. Mirza, O., Uy, B. "Behaviour of composite beam-column flush end-plate connections subjected to low-probability, high-consequence loading". *Engineering Structures*, 33(2), 2011, pp. 647-662.
22. Sun, Z., Siringoringomm, D. M., Fujino, Y. "Load-carrying capacity evaluation of girder bridge using moving vehicle". *Engineering Structures*, 229, 2021, pp. 111645.
23. Moon, H. S., Ok, S., Chun, P. J. "Artificial neural network for vertical displacement prediction of a bridge from strains (part 1): girder bridge under moving vehicles". *Applied Sciences-Basel*, 9(14), 2019, pp. 2881.
24. Muho, E. V., Beskou, N. D. "Dynamic response of an isotropic elastic half-plane with shear modulus varying with depth to a load moving on its surface". *Transportation Geotechnics*, 20, 2019, pp. 100248
25. Pegios, I. P., Papargyri, B. S., Zhou, Y. "Steady-state dynamic response of a gradient elastic half-plane to a load moving on its surface with constant speed". *Archive of Applied Mechanics*, 89(9), 2019, pp. 1809-1824.
26. Wen, S. R., Wu, Z. J., Lu, N. L. "High-precision solution to the moving load problem using an improved spectral element method". *Acta Mechanica Sinica*, 34(1), 2018, pp. 68-81.
27. Elnashar, G., Bhat, R. B., Sedaghati, R. "Modeling and dynamic analysis of a vehicle-flexible pavement coupled system subjected to road surface excitation". *Journal of Mechanical Science and Technology*, 33(7), 2019, pp. 3115-3125.
28. Gwon, S. G., Choi, D. H. "Static and dynamic analyses of a suspension bridge with three-dimensionally curved main cables using a continuum model". *Engineering Structures*, 161, 2015, pp. 250-264.
29. Yan, Z. Y., Chen, E. L., Wang, Z., Si, C. D. "Research on mesoscopic response of asphalt pavement structure under vibration load". *Shock and Vibration*, 2019, 2019, pp. 2620305.
30. Yu, H. L., Wang, B., Li, Y. L. "Road vehicle-bridge interaction considering varied vehicle speed based on convenient combination of simulink and ansys". *Shock and Vibration*, 2018, 2018, pp. 1389628.